IEEE Wireless and Microwave Technology Conference (WAMICON 2017)
Cocoa Beach FL, USA, 24–25 April, 2017

SOCP Design of Monopulse Sum and Difference Beams for a Uniform Circular Array

W. Mark Dorsey
wmdorsey@vt.edu
Radar Division

IEEE
Senior Members
Naval Research Laboratory
Washington DC, USA

Jeffrey O. Coleman
http://alum.mit.edu/www/jeffc
Radar Division (retired)

***Abstract*—Classical sum and difference beams for angle measurement in amplitude-comparison monopulse systems are constructed by adding and subtracting narrow beams slightly offset in pointing angle. Here instead beams with sum and difference behavior in azimuth are synthesized using second-order cone programs applicable to any array for which embedded complex element patterns are known. The computational example here is specific to a uniform circular array (UCA) because it uses embedded element patterns obtained by rotating a prototype pattern through angles uniformly spaced around the circle. That prototype was computed through electromagnetic simulation of a UCA of simple patch elements.**

I. Introduction

A second-order cone program (SOCP) is a linear program with the addition of second-order cone constraints of the form $\|\mathbf{v}\| \le b$, where vector $\mathbf{v}$ and bound b are affine in the variables being optimized and where the norm is Euclidean. In digital-filter [1], [2] and array [3], [4], [5], [6], [7] optimization, such cone constraints are used routinely to bound energies and complex magnitudes.

Monopulse angle measurement's sum and difference beams are named after their classic construction that adds and subtracts narrow beams slightly offset in pointing angle. Here instead we formulate SOCPs to synthesize sum and difference beams—we retain the names—directly. The Section III computational examples are for a uniform circular array (UCA), but the SOCP formulation of Section II applies to any array setting for which embedded element patterns are known.

This is the simplest of preliminary studies, not a thorough examination of the topic. It's aim is to suggest a direction and general approach for future work.

II. The Second-Order Cone Programs

After the next section's background review to clarify notation, Sections B and C present SOCPs to optimize first the sum and then the difference pattern. It may help in following the latter sections to look ahead to the plots of Section III.

A. Standard background material but in our notation

A plane wave incident with real wavenumber vector $-2\pi\mathbf{k}$ and complex vector amplitude $\vec{p}$ has frequency $c\|\mathbf{k}\|$ with vector $\mathbf{k}$ pointing in the direction of arrival (DOA). Complex vector antenna pattern $\vec{f}(\mathbf{k})$ depends on DOA and frequency through $\mathbf{k}$, and the antenna output is complex three-space inner product $\langle \vec{p}, \vec{f}^*(\mathbf{k})\rangle$, which sums the Cartesian components of $\vec{p}$ scaled by the Cartesian components of $\vec{f}(\mathbf{k})$. If orthogonal dimensionless complex unit vectors $\vec{c}$ and $\vec{x}$ define co- and cross-polarization in a way dependent on DOA and normal to $\vec{p}$, pattern $\vec{f}(\mathbf{k})$ can harmlessly be projected onto the span of their conjugates as

$$\vec{f}(\mathbf{k}) = f_c(\mathbf{k})\,\vec{c}^{\,*} + f_x(\mathbf{k})\,\vec{x}^{\,*}$$

where complex scalar coordinates $f_c(\mathbf{k})$ and $f_x(\mathbf{k})$ are the co- and cross-pol patterns, and the antenna output is

$$\langle \text{output}\rangle = \langle \vec{p}, \vec{f}^*(\mathbf{k})\rangle = f_c(\mathbf{k})\,\langle \vec{p}, \vec{c}\,\rangle + f_x(\mathbf{k})\,\langle \vec{p}, \vec{x}\,\rangle.$$

The inner products are co- and cross-pol signal amplitudes. (One could define co- and cross-pol unit vectors $\vec{c}$ and $\vec{x}$ as the conjugates of those implicitly defined here. Its a question of whether one interprets them as the axes onto which signal is projected or onto which the antenna pattern is projected.)

Using conjugated complex weights $\{w_i^*\}$, an array of M elements with embedded element patterns $\{\vec{f}_i(\mathbf{k})\}$ has output

$$\langle \text{output}\rangle = \sum_{i=1}^{M} w_i^* \langle \vec{p}, \vec{f}_i^*(\mathbf{k})\rangle = \left\langle \vec{p}, \left(\sum_{i=1}^{M} w_i^*\,\vec{f}_i(\mathbf{k})\right)^* \right\rangle.$$

Let array pattern $\vec{F}(\mathbf{k})$ be the parenthesized sum on the right above and decompose it into co- and cross-pol components as

$$\vec{F}(\mathbf{k}) = F_c(\mathbf{k})\,\vec{c}^{\,*} + F_x(\mathbf{k})\,\vec{x}^{\,*}, \tag{1}$$

$$F_c(\mathbf{k}) = \sum_{i=1}^{M} w_i^* f_{ci}(\mathbf{k}), \quad F_x(\mathbf{k}) = \sum_{i=1}^{M} w_i^* f_{xi}(\mathbf{k}). \tag{2}$$

If $\mathbf{f}(\mathbf{k}) \triangleq [f_{ci}(\mathbf{k})]$ and $\mathbf{w} \triangleq [w_i]$ define complex column M vectors containing embedded co-pol element patterns and weights respectively, the co-pol array pattern becomes $F_c(\mathbf{k}) = \langle \mathbf{f}(\mathbf{k}), \mathbf{w}\rangle = \mathbf{w}^H\mathbf{f}(\mathbf{k})$, an inner product of complex M vectors. Given a co-pol incident signal with $\vec{p} = p\vec{c}$ for some complex amplitude p, the array output is $\langle \vec{p}, \vec{F}^*(\mathbf{k})\rangle = pF_c(\mathbf{k})$ by (1).

In an obvious extension of notation, using the weight vectors $\mathbf{w}_\Sigma$ and $\mathbf{w}_\Delta$ in the following sections for sum and difference beams yields array patterns $\vec{F}_\Sigma(\mathbf{k})$ and $\vec{F}_\Delta(\mathbf{k})$, co-pol patterns $F_{\Sigma c}(\mathbf{k})$ and $F_{\Delta c}(\mathbf{k})$, and array outputs $pF_{\Sigma c}(\mathbf{k})$ and $pF_{\Delta c}(\mathbf{k})$ for amplitude p co-pol signals. The *monopulse ratio* is either the ratio of difference- and sum-beam outputs, again assuming a co-pol signal, or the ratio of those same co-pol patterns:

$$\langle \text{monopulse ratio}\rangle \triangleq \frac{pF_{\Delta c}(\mathbf{k})}{pF_{\Sigma c}(\mathbf{k})} = \frac{F_{\Delta c}(\mathbf{k})}{F_{\Sigma c}(\mathbf{k})}.$$

Work supported by the InTop program of the Office of Naval Research.

The cancellation of the complex amplitude p on the right is of course why the ratio on the left is used in angle estimation.

We ignore the cross-pol signal components and patterns in the monopulse angle estimation. This is of course not entirely appropriate, and a less preliminary exploration of the topic would need to consider them carefully.

B. Design the sum beam using an established SOCP approach

When identical individual LNAs set the noise figures of the element outputs of a receive array of M elements, this SOCP from [7] enforces a polarization-insensitive bound δ on sidelobe magnitudes at some number s_{max} values of vector $\mathbf{k}$ that are closely spaced across the sidelobe region while maximizing receive co-pol SNR at the $\mathbf{k} = \mathbf{k}_{\text{mb}}$ mainbeam center by minimizing taper loss $20 \log_{10} \Lambda_\Sigma$.

$$\begin{aligned} &\textit{Optimize} \text{ real variable } \Lambda_\Sigma \text{ and complex vector } \mathbf{w}_\Sigma \\ &\textit{to minimize } \Lambda_\Sigma \\ &\textit{subject to} \text{ noise constraint } \|\mathbf{w}_\Sigma\| \|\mathbf{f}(\mathbf{k}_{\text{mb}})\| \le \Lambda_\Sigma, \\ &\qquad \text{mainbeam constraint } \operatorname{Re}(\langle \mathbf{f}(\mathbf{k}_{\text{mb}}), \mathbf{w}_\Sigma \rangle) \ge 1, \text{ and} \\ &\qquad \text{point bounds } \|\vec{F}_\Sigma(\mathbf{k}_s)\| \le \delta \text{ for } s = 1, 2, \ldots, s_{\text{max}}. \end{aligned} \tag{3}$$

The mainbeam constraint is a linear inequality bounding an inner product in complex M space, and the noise constraint is a second-order cone using a norm in that same space. Each point bound is a second-order cone using a norm in complex three-space. Computing the point-bound norms uses, from (1),

$$\|\vec{F}_\Sigma(\mathbf{k})\|^2 = |F_{\Sigma c}(\mathbf{k})|^2 + |F_{\Sigma x}(\mathbf{k})|^2.$$

C. A difference-beam SOCP adapted from the sum-beam one

The following difference-beam SOCP is similar to sum-beam SOCP (3) except in the mainbeam area. In fact the sidelobes are constrained exactly as before.

$$\begin{aligned} &\textit{Optimize} \text{ real variable } \rho \text{ and complex vector } \mathbf{w}_\Delta \\ &\textit{to minimize } -\rho \\ &\textit{subject to} \text{ noise constraint } \|\mathbf{w}_\Delta\| \|\mathbf{f}(\mathbf{k}_{\text{mb}})\| \le \Lambda_\Sigma, \\ &\qquad \text{mainbeam null constraint } \langle \mathbf{f}(\mathbf{k}_{\text{mb}}), \mathbf{w}_\Delta \rangle = 0, \\ &\qquad \text{mainbeam slope constraint } \operatorname{Re}\big(\langle \mathbf{f}'(\mathbf{k}_{\text{mb}}), \mathbf{w}_\Delta \rangle\big) \ge \rho, \\ &\qquad \text{point bounds } \|\vec{F}_\Delta(\mathbf{k}_s)\| \le \delta \text{ for } s = 1, 2, \ldots, s_{\text{max}}. \end{aligned} \tag{4}$$

The single mainbeam constraint in (3) is here replaced with two new constraints. The first is an equality constraint to create a null at mainbeam center.[1] The second lower bounds the derivative of the real part of the co-pol pattern, at mainbeam center, with a new optimized variable ρ using equivalence

$$\begin{aligned} \frac{d}{d\theta} \operatorname{Re}(F_{\Delta c}(\mathbf{k}(\theta))) &= \operatorname{Re}\left(\sum_{i=1}^{M} w_{\Delta i}^* \frac{d f_{ci}(\mathbf{k}(\theta))}{d\theta} \right) \\ &= \operatorname{Re}\big(\langle \mathbf{f}'(\mathbf{k}_{\text{mb}}), \mathbf{w}_\Delta \rangle \big), \\ \mathbf{f}'(\mathbf{k}_{\text{mb}}) &\triangleq \left[\frac{d f_{ci}(\mathbf{k}(\theta))}{d\theta} \right]_{\theta=0} \end{aligned}$$

[1] Alternatively, a complex quantity C that is affine in the optimized variables like that mainbeam sample can be made tiny with rank-two second order cone $|C| \le \epsilon$ rather than be made zero with linear equality constraint $C = 0$. Freeing up of two (real and imaginary parts) degrees of freedom in that way, not tested here, sometimes results in modestly improved optimization performance.

using (2) with $\mathbf{k}(\theta)$ denoting $\mathbf{k}_{\text{mb}}$ rotated by azimuth angle θ and with prime denoting $d/d\theta$ of a function of $\mathbf{k}(\theta)$. To then maximize the slope of the real part of the pattern sample, we minimize $-\rho$ to maximize ρ. In practice it is quite adequate to approximate the derivatives numerically.

Zeroing the slope of the imaginary part of the mainbeam-center co-pol difference pattern is not needed, as rotating the weights in unison in the complex plane by replacing $\mathbf{w}_\Delta$ with $\mathrm{e}^{j\zeta} \mathbf{w}_\Delta$ changes no other constraint. As optimization rotates the weights to maximize the slope's real part then, the imaginary part of that slope is zeroed. Making the imaginary part zero at the center in both value and slope makes it effectively zero in value across the central part of the mainbeam and so makes that part of the pattern real. Through a similar mechanism, the objective and mainbeam constraint in sum-beam SOCP (2) makes that part of the sum pattern real as well.

With both patterns real near mainbeam center, maximizing the difference-beam slope at the center indirectly maximizes the slope of the monopulse ratio there as well. To see this, note that we now have $F_{\Sigma c}(\mathbf{k}(0)) = 1$, $F_{\Delta c}(\mathbf{k}(0)) = 0$, and if sidelobe constraints in sum-beam SOCP (2) are located symmetrically with respect to mainlobe center as is typical, $F'_{\Sigma c}(\mathbf{k}(0)) \approx 0$ as well. The monopulse-ratio slope is then

$$\begin{aligned} &\left[\frac{d \operatorname{Re}\left(\dfrac{F_{\Delta c}(\mathbf{k}(\theta))}{F_{\Sigma c}(\mathbf{k}(\theta))} \right)}{d\theta} \right]_{\theta=0} \\ &\quad = \frac{F'_{\Delta c}(\mathbf{k}(0))\, F_{\Sigma c}(\mathbf{k}(0)) - F'_{\Sigma c}(\mathbf{k}(0))\, F_{\Delta c}(\mathbf{k}(0))}{F^2_{\Sigma c}(\mathbf{k}(0))} \\ &\quad = \frac{F'_{\Delta c}(\mathbf{k}(0)) \times 1 - 0 \times 0}{1} = F'_{\Delta c}(\mathbf{k}(0)). \end{aligned}$$

Won't pushing upward on the slope at mainbeam center just push ρ and the weights to infinity together? It would indeed if we used a new noise-level optimization variable Λ_Δ on the right side of the noise constraint to parallel the construction in sum-beam SOCP (2). So instead we use the sum beam's noise bound Λ_Σ, which was already optimized and is now constant. This also equates the sum and difference outputs' noise levels.

III. Simulation

A. Array geometry and element design

Here we illustrate SOCP design of UCA sum and difference beams for monopulse measurement of emitter azimuth using the UCA geometry from [8] shown in Fig. 1. We obtained the embedded co-pol complex pattern of one element using simulation in CST Microwave Studio, with that element driven and the others terminated [9], and we then rotated that first pattern in azimuth to create the other element patterns. The magnitude of that first, simulated pattern appears in Fig. 2. The large number of elements—relatively close spacing—simplifies beam steering [8], but one could certainly economize and use fewer elements along the same array circumference by omitting steering and simply drawing on a library of sum and difference patterns designed with the current approach for closely spaced mainbeam directions.

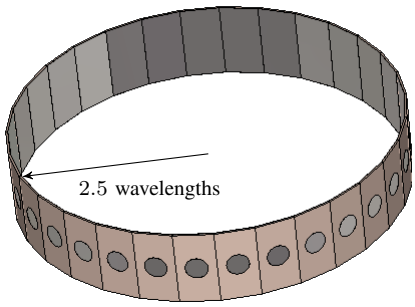

Fig. 1. The UCA design features $M = 49$ vertically polarized patch elements. Circumferential spacing of 2.5 wavelengths $\times 2\pi/M$ between element centers is approximately 0.32 wavelengths.

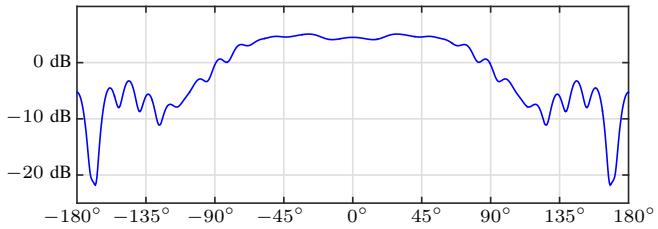

Fig. 2. Magnitude of complex co-pol embedded element pattern $f_{c1}(\mathbf{k}(\theta))$, which was linearly interpolated from complex samples computed at 0.5° intervals using electromagnetic simulation. Pattern elevation was fixed at 0°.

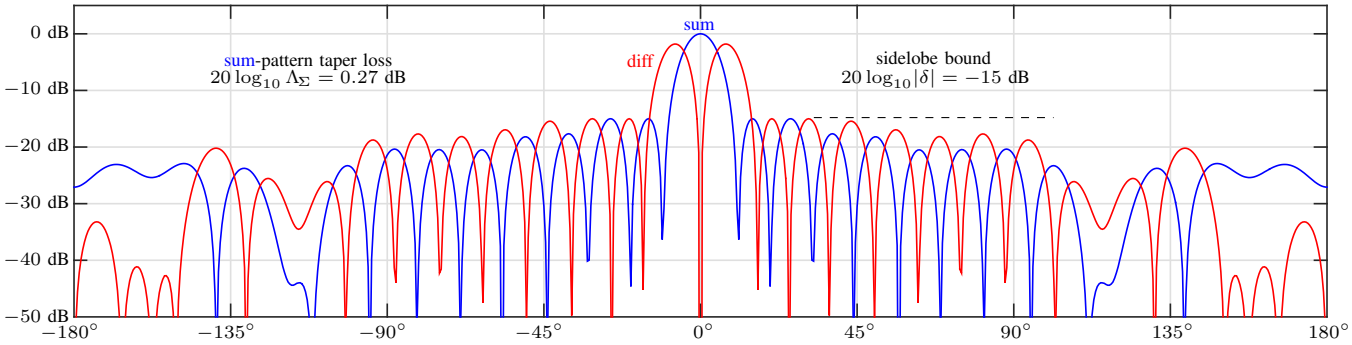

Fig. 3. Sum and difference pattern magnitudes for a $M = 49$ element UCA.

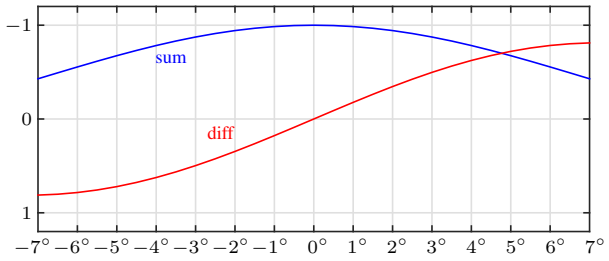

Fig. 4. Sum and difference patterns of Fig. 3 on a linear scale.

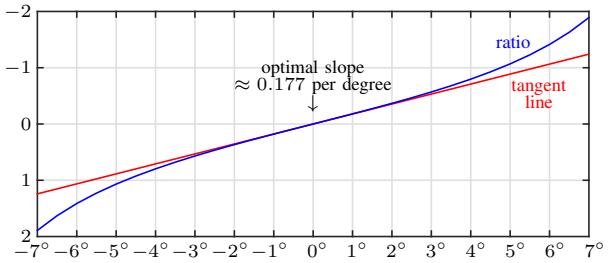

Fig. 5. The ratio of the Fig. 4 difference and sum patterns.

B. The optimized patterns

Fig. 3 plots the magnitudes of sum and difference co-pol patterns designed with SOCPs (3) and (4) using the element patterns discussed above. Mainbeam defining parameter $\mathbf{k}_{\text{mb}}$ points at zero elevation with azimuth aligned with the center of element 1, but further computational experiments verified that its azimuth can be set arbitrarily with substantially similar results. These plots, like those to come, are versus θ, the azimuth deviation from the direction of $\mathbf{k}_{\text{mb}}$.

The SOCPs were solved in matlab using the Opt toolbox [2] for high-level problem setup and using the free SeDuMi solver [10], [11] for actual optimization. (The free SDPT3 solver [12], [13], [14] would be equally suitable.) Elapsed optimization times for sum and difference patterns were 649 ms and 263 ms respectively on a late-2013 notebook computer.

The sum-pattern taper loss in Fig. 3 is controlled indirectly through sidelobe-bound parameter δ in SOCPs (3) and (4). Less sidelobe suppression lowers taper loss, while no sidelobe suppression at all—point-bound constraints removed or δ set so high as to make the those constraints inactive—reduces the taper loss to 0 dB. More sidelobe suppression than used here rapidly increases taper loss. As discussed in [7], it is straightforward to modify SOCP (3) to instead explicitly bound the taper loss and maximize sidelobe suppression.

The Fig. 3 sidelobe bound was enforced for $|\theta| \geq 15°$ and $|\theta| \geq 18°$ for the sum and difference pattern respectively, with those $|\theta|$ bounds hand chosen to control sidelobes without touching the main beams. In both cases point bounds were placed at half-degree intervals out to $\pm 45°$ degree maximum. Fig. 3 shows that the outer point-bound constraints were not active, so while these bounds could have been placed all the way out to $\pm 180°$, the extra bounds would have been inactive.

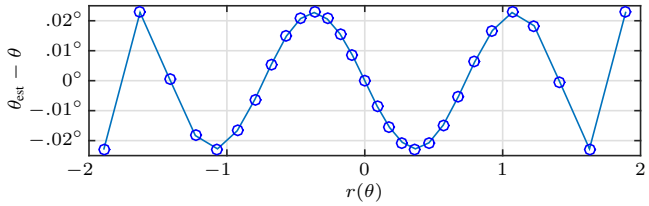

Fig. 6. Correction error $\theta_{\text{est}} - \theta$ versus monopulse ratio $r(\theta)$ when estimate θ_{est} is given by example three-term correction polynomial (5).

Both patterns are essentially real: neither of their imaginary parts exceeded 3×10^{-4} in magnitude for any angle θ. The complex correlation coefficient between the noise components of the sum and difference outputs is given by

$$\frac{\langle \mathbf{w}_\Sigma, \mathbf{w}_\Delta \rangle}{\|\mathbf{w}_\Sigma\| \|\mathbf{w}_\Delta\|}$$

and turns out to be zero here to machine precision.

C. The monopulse ratio

The mainbeam-center portions of the real parts of the sum and difference patterns of Fig. 3 are shown on a linear scale in Fig. 4. The monopulse ratio, the difference pattern over the sum pattern, is shown in Fig. 5 with, for comparison, a line tangent at the origin.

The nonlinearity of the ratio versus θ could be addressed in practice in a variety of ways. Certainly the sum beam could simply be widened to improve the ratio's linearity, say by replacing the one mainbeam constraint with a constraint pair straddling the origin. Alternatively, some sort of linearizing correction function could be applied to the ratio, perhaps using interpolation from a lookup table.

Another possibility is to design a correction polynomial. Representing the Fig. 5 ratio by $r = f(\theta)$, we can construct approximate inversion $\theta_{\text{est}} \approx f^{-1}(r)$ using a simple linear program to set θ_{est} to an odd-order polynomial in r designed to yield an approximately equiripple error:

$$\begin{aligned} &\textit{Optimize} \text{ real variables } a, b, c, \text{ and } d \\ &\textit{to minimize } d \\ &\textit{subject to} \text{ bound } \left|\big(ar^5(\theta_i) + br^3(\theta_i) + cr(\theta_i)\big) - \theta_i\right| \le d \\ &\qquad \text{for } i = 1, 2, \ldots, i_{\max}. \end{aligned}$$

The parenthesized polynomial in $r(\theta)$ is optimized by minimizing bound d on the absolute value of the approximation error sampled at $\theta = \theta_i$ for $i = 1, \ldots, i_{\max}$.

This linear program was solved with angles $\theta_1, \ldots, \theta_{\max}$ placed at $0.5°$ intervals from $0°$ to $7°$ and to obtain polynomial

$$\theta_{\text{est}} \triangleq 0.080609\, r^5 - 0.78659\, r^3 + 5.4950\, r \qquad (5)$$

with error bound $d = |\theta_{\text{est}} - \theta| \le 0.023°$. The resulting correction error at ratio values $r(\theta_i)$ is marked with circles ○ in Fig. 6. The nonsmooth behavior as $|r(\theta)|$ approaches 2 indicates that samples θ_i should be spaced more closely to obtain a realistic design. Crude spacing here serves to warn.

IV. Conclusions

UCA sum and difference beams for monopulse measurement of the azimuth of a co-pol emitter are easily synthesized using second-order cone programming. They can be synthesized for any specific pointing direction or, if the center-to-center element spacing is sufficiently small, synthesized for one direction only and then steered to the direction desired in practice using a recent Fourier-series approach [8].

Appropriate for future work would be examination of the effects of polarization mismatch on the angle measurement. It may be necessary in the end to use dual-pol elements and modify the SOCPs to synthesize mainbeam patterns in an elevation-aware manner.

References

[1] J. O. Coleman and D. P. Scholnik, "Design of nonlinear-phase FIR filters with second-order cone programming," in *Proc. 42nd Midwest Symp. on Circuits and Systems*, Aug. 1999, pp. 409–412, vol. 1.

[2] J. O. Coleman, D. P. Scholnik, and J. J. Brandriss, "A specification language for the optimal design of exotic FIR filters with second-order cone programs," in *Proc. 36th Asilomar Conf. on Signals, Systems and Computers*, Nov. 2002, pp. 341–345, vol. 1, note the IEEE Xplore pdf is poor, so seeking out a preprint is advised.

[3] J. O. Coleman, D. P. Scholnik, and P. E. Cahill, "Synthesis of a polarization-controlled pattern for a wideband array by solving a second-order cone program," in *Proc. IEEE Antennas and Propagation Society Int'l Symp.*, Jul. 2005, pp. 437–440, vol. 2B.

[4] D. P. Scholnik and J. O. Coleman, "Optimal array-pattern synthesis for wideband digital transmit arrays," *IEEE J. Sel. Topics Signal Process.*, vol. 1, no. 4, pp. 660–677, Dec. 2007.

[5] J. O. Coleman, "Nonseparable Nth-band filters as overlapping-subarray tapers," in *Proc. IEEE Radar Conf.*, May 2011, pp. 141–146.

[6] W. M. Dorsey, J. O. Coleman, R. W. Kindt, and R. Mital, "Second-order cone programming for scan-plane reconstruction for the wavelength-scaled array," *IEEE Trans. Antennas Propag.*, vol. 62, no. 5, pp. 2826–2831, May 2014.

[7] W. Dorsey, J. Coleman, and W. Pickles, "Uniform circular array pattern synthesis using second-order cone programming," *IET Microwaves, Antennas, and Prop.*, vol. 9, no. 8, pp. 723–727, 2015.

[8] J. O. Coleman and W. M. Dorsey, "Phase-shift steer a uniform circular array in the Fourier-series domain," in *Proc. IEEE Wireless and Microwave Technology Conf.*, Apr. 2017, submitted.

[9] D. F. Kelley and W. L. Stutzman, "Array antenna pattern modeling methods that include mutual coupling effects," *IEEE Transactions on Antennas and Propagation*, vol. 41, no. 12, pp. 1625–1632, Dec. 1993.

[10] J. F. Sturm, "Using SeDuMi 1.02, a Matlab toolbox for optimization over symmetric cones," *Optimization methods and software*, vol. 11–12, pp. 625–653 (versions 1.02/1.03), 1999, updated in 2001 for version 1.05. [Online]. Available: http://www.optimization-online.org/DB_HTML/2001/10/395.html

[11] Imre Pólik and Tamás Terlaky. "SeDuMi 1.3." Cor@l Lab: Computational Optimization Research at Lehigh. Lab website: http://coral.ie.lehigh.edu/. [Online]. Available: http://sedumi.ie.lehigh.edu/

[12] K.-C. Toh, M. J. Todd, and R. H. Tütüncü, "SDPT3—a Matlab software package for semidefinite programming," *Optimization methods and software*, vol. 11, pp. 545–581, 1999. [Online]. Available: http://www.tandfonline.com/doi/abs/10.1080/10556789908805762

[13] R. H. Tütüncü, K.-C. Toh, and M. J. Todd, "Solving semidefinite-quadratic-linear programs using SDPT3," *Math. Program. Ser. B*, vol. 95, no. 2, pp. 189–217, 2003. [Online]. Available: http://dx.doi.org/10.1007/s10107-002-0347-5

[14] K.-C. Toh, M. J. Todd, and R. H. Tütüncü. (2006, Jul. 17) "SDPT3 version 4.0—a MATLAB software for semidefinite-quadratic-linear programming." Dept. of Mathematics, National Univ. of Singapore. [Online]. Available: http://www.math.nus.edu.sg/~mattohkc/sdpt3.html